A gate-tunable graphene Josephson parametric amplifier

Guilliam Butseraen, Arpit Ranadive, Nicolas Aparicio, Kazi Rafsanjani Amin, Abhishek Juyal, Martina Esposito, Kenji Watanabe, Takashi Taniguchi, Nicolas Roch, François Lefloch, et al.

A gate-tunable graphene Josephson parametric amplifier

Guilliam Butseraen,[1] Arpit Ranadive,[1] Nicolas Aparicio,[1] Kazi Rafsanjani Amin,[1,2] Abhishek Juyal,[1] Martina Esposito,[1,3] Kenji Watanabe,[4] Takashi Taniguchi,[5] Nicolas Roch,[1] François Lefloch,[6] and Julien Renard[1,*]

[1] *Univ. Grenoble Alpes, CNRS, Grenoble INP, Institut Néel, 38000 Grenoble, France*

[2] *Univ. Grenoble Alpes, CEA, LETI, 38000 Grenoble, France*

[3] *CNR-SPIN Complesso di Monte S. Angelo, via Cintia, Napoli 80126, Italy*

[4] *Research Center for Functional Materials, National Institute for Materials Science, 1-1 Namiki, Tsukuba 305-0044, Japan*

[5] *International Center for Materials Nanoarchitectonics, National Institute for Materials Science, 1-1 Namiki, Tsukuba 305-0044, Japan*

[6] *Univ. Grenoble Alpes, CEA, Grenoble INP, IRIG-PHELIQS, 38000 Grenoble, France*

Introductory paragraph

With a large portfolio of elemental quantum components, superconducting quantum circuits have contributed to advances in microwave quantum optics [1]. Of these elements, quantum-limited parametric amplifiers [2–4] are essential for low noise readout of quantum systems whose energy range is intrinsically low (tens of μeV) [5, 6]. They are also used to generate non classical states of light that can be a resource for quantum enhanced detection [7]. Superconducting parametric amplifiers, like quantum bits, typically utilize a Josephson junction as a source of magnetically tunable and dissipation-free nonlinearity. In recent years, efforts have been made to introduce semiconductor weak links as electrically tunable nonlinear elements, with demonstrations of microwave resonators and quantum bits using semiconductor nanowires [8, 9], a two dimensional electron gas [10], carbon nanotubes [11] and graphene [12, 13]. However, given the challenge of balancing nonlinearity, dissipation, participation, and energy scale, parametric amplifiers have not yet been implemented with a semiconductor weak link. Here we demonstrate a parametric amplifier leveraging a graphene Josephson junction and show that its working frequency is widely tunable with a gate voltage. We report gain exceeding 20 dB and noise performance close to the standard quantum limit. Our results expand the toolset for electrically tunable superconducting quantum circuits. They also offer opportunities for the development of quantum technologies such as quantum computing, quantum sensing and for fundamental science [14].

Main text

In Fig. 1a, we present the schematic of the designed parametric amplifier. The graphene Josephson junction is embedded at the voltage node of a half-wave microwave resonator with resonant frequency $\frac{\omega_0}{2\pi}$=6.44 GHz (measured experimentally in the absence of the junction, see Extended Data Fig. 1 and supplementary information, section II). It provides the lossless nonlinearity required to perform wave mixing and necessary for a low noise amplification

* julien.renard@neel.cnrs.fr

process [15].

In Fig. 1b, we present the DC resistance of the device as a function of the gate voltage (V_g) and bias current (I_b). At low DC bias current, the device resistance vanishes and a Josephson supercurrent can flow in the graphene. Above the critical current I_c, dissipation kicks in, and as a result, we observe a non-zero differential resistance. We observe that the critical current strongly depends on the gate voltage and can be varied from 100 nA up to more than 1.3 μA. Such large critical current and the value of the $R_n \times I_c$ product ($R_n \times I_c \sim 1.4\Delta$, where R_n and Δ are the normal state resistance and the induced superconducting gap, see Extended Data Fig. 2 and supplementary information, section IV) proves the high quality of the junction [16].

We also observe that the gate voltage modifies the microwave resonance frequency (Fig. 1c) [12], that is measured with a vector network analyzer (VNA) in the low power limit. For gate voltages corresponding to a high critical current, the frequency is close to the measured bare resonance frequency $f_0 = \frac{\omega_0}{2\pi} = 6.44$ GHz. For lower critical currents, the frequency is reduced. This is a direct consequence of the relationship between the critical current and the Josephson inductance L_J . Assuming for simplicity a sinusoidal current phase relation and zero phase bias across the junction, we have $L_J = \frac{\Phi_0}{2\pi I_c}$, where $\Phi_0 = \frac{h}{2e}$ is the magnetic flux quantum. A modulation of I_c with V_g thus translates into a modification of L_J resulting in a change of the resonance frequency: $\omega_r(V_g) = \frac{1}{\sqrt{(L_0+L_J(V_g))C}}$, where L_0 is the resonator inductance in the absence of the Josephson junction and C the total capacitance.

In Fig. 1d, we compare the prediction of the resonance frequency given by this simple equivalent lumped element model with its experimental determination using microwave measurements (see supplementary information, section IV), showing a good agreement between the two. The discrepancies at low frequencies are attributed to an underestimation of the critical current in the DC experiment, which rather measures the switching current and can thus overestimate the Josephson inductance. At high frequency, on the other hand, the mismatch can be attributed to deviations of the current phase relation from its assumed sinusoidal form. In this region, our data indicate a larger inductance than the one predicted by the critical current (see supplementary information, section IV). This would point towards a forward skewed current phase relation, which has been observed in highly transparent graphene Josephson junctions [17–19].

In Fig. 2a, we present the microwave reflection (S_{11}) of the device at V_g=15 V, with no DC bias current, for different input powers to study the nonlinear regime. The main feature that we observe is a decrease of the resonance frequency when the probe power increases, due to the Kerr nonlinearity. In addition, we notice that the magnitude of the reflection dip increases slightly with power. This is a signature of nonlinear losses that are not observed in usual tunnel Josephson junctions. Nonlinear losses have been shown to exist in graphene Josephson junctions and have been attributed to the presence of subgap states inside the induced superconducting gap [18, 19], which are absent in tunnel junctions. The position and density of these subgap states is influenced by the exact geometry of the junction [12] and its optimization should allow to mitigate their effect in the microwave range of interest.

To model the behaviour of our device we use the following nonlinear Hamiltonian, typical for such superconducting circuits with an embedded Josephson junction [20]:

$$H = \hbar\omega_r A^\dagger A + \hbar\frac{K}{2}(A^\dagger)^2 A^2 \tag{1}$$

where ω_r is the angular resonance frequency which in our case can be tuned with V_g, K is the Kerr nonlinearity and A (resp. $A^\dagger$) the annihilation (resp. creation) operator of resonator photons. The resonator presents some internal losses (rate $2\gamma_2$) and is coupled to an input/output port for measurement (coupling rate $2\gamma_1$). We also include a nonlinear loss term, in the form of two photon losses (rate $2\gamma_3$) [20].

The full nonlinear response of the system can then be calculated using input-output theory [20] (see supplementary information, section V) showing a good agreement with the experiment (see Fig. 2b). This allows us to extract the parameters of our nonlinear resonator (see Fig. 2). We note that the agreement between the model and the experiment depends on the gate voltage. For some gate voltages we see that the model is not well suited to describe the system (see supplementary information, section V). We can formulate several hypothesis to account for this. First, this could come from the fact that higher order terms of the nonlinearity are neglected in the model. Another possibility could be that the model assumes a sinusoidal current phase relation. With a non-sinusoidal current phase relation, one would need to include additional terms in the nonlinearity, in particular a cubic term that could have a contribution comparable to the quartic one. Such analysis nevertheless goes beyond the scope of the current study. Finally the presence of nonlinear losses in the device is only included to first order. The exact power dependance of the losses is likely to

be more complicated and a more realistic model should be developed to take into account the detailed nature of the nonlinear losses.

The estimated Kerr nonlinearity in the device is weak, with $\frac{|K|}{\omega_0} \sim 10^{-4}$, which is typical for Josephson parametric amplifiers [2]. Finally, above a threshold power, the resonator bifurcates and enters a bistable regime, characteristic of such a nonlinear circuit.

We will now focus on the regime of interest for parametric amplification, that is slightly below bifurcation. Here, two signals are sent to the input of the device: a strong pump tone (frequency f_p) and a weak probe tone (frequency f_s), whose reflection is measured with a VNA. Both signals frequencies are chosen close to the resonance frequency of the resonator and we have the relation $2f_p = f_s + f_i$, where f_i is the frequency of the complementary idler mode. We are thus in a four-wave mixing scheme of amplification which is the one expected from the Hamiltonian in Eq 1. In Fig. 3a, we see the effect of the pump on the magnitude of the reflection coefficient; in the presence of the pump, the probe signal is amplified by as much as 22 dB. This is the signature of parametric amplification. Amplification is present in a small frequency range near the pump frequency, limited by the resonator bandwidth. We extract a gain-bandwidth product of 33 MHz, which is typical for resonant Josephson parametric amplifier and mainly set by the coupling to the measurement port. The slightly larger gain-bandwidth product than the one that could be inferred from the system parameters (see Fig. 2) comes from a small change of setpoint between the two measurements.

In Fig. 3a, we compare the experimentally measured gain with the one predicted by the input-output model using the parameters extracted from the one-tone measurement (see Fig 2). We see that the gain profile is qualitatively described by the formalism of Josephson parametric amplifiers [20] (see supplementary information, section V, for more details about the modeling of the gain).

In a resonant Josephson parametric amplifier, amplification can typically be achieved only in a narrow frequency range close to the resonance frequency of the superconducting resonator. In our device, the resonance frequency can be tuned with a simple gate voltage as we reported in Fig. 1 . We now explore the possibility to realize amplification in a broad frequency range and present the main result of this work. In Fig. 3b, we show gain profiles measured across the full range of tunability of the resonance frequency. For each frequency, set by a chosen V_g, pump frequency and power are optimized accordingly. We see that we can have a large gain (>15dB) in a frequency range of about 1 GHz, i.e. more than

100× the bandwidth of the amplifier. This gives interesting perspectives for qubit readout as the amplifier could be used to selectively address superconducting circuits at different operating frequencies by choosing the gate voltage. A gate voltage tuning has advantages compared to traditional magnetic flux tuning obtained in SQUID as the local character of the electrical control will suppress crosstalk issues between different parts of the device. But such advantage will really materialize when fast gate voltage tuning of the amplifier can be demonstrated with the use of an efficient gating design and standard large bandwidth control techniques.

Variations in the apparent gain and deviations from an ideal Lorentzian shape are attributed to non-optimal pump parameters that can come from gate voltage instability (see supplementary information, section III). Nevertheless, maximum gains are expected to be reduced when the graphene Josephson junction nonlinearity is not optimal, for instance too large, close to the Dirac point, i.e. at low frequency. We also observe that the nonlinear losses seem to increase at high frequency, above 6.2 GHz, which could explain the lower gains in this region. While identifying the exact mechanism to explain the losses would require further investigations, it is possible that it comes from the reduced non-linearity at higher frequency. The reduction of the non-linearity imposes that a larger working power is necessary to reach gain. Such larger working power, which in a simple picture means an exploration of the current-phase away from zero phase, could be the reason of the apparent larger losses.

Having demonstrated large gain and tunability we now turn to two essential characteristics of a superconducting parametric amplifier: dynamic range and noise. The dynamic range indicates the input power that can be sent to the amplifier before the gain is appreciably reduced. To measure it experimentally, we measure the gain as a function of probe power for fixed frequency and pump power. In Fig.4a, we see that the gain is reduced by 1 dB for an input power of -123 ±3 dBm: this is the 1 dB compression point P_{1dB} for our device. Such a value is comparable to the best values obtained with single Josephson junction JPA [21]. It is intrinsically related to the junction nonlinearity, critical current and the exact resonator design. This can be improved in future realizations by using arrays of junctions with larger critical currents [22].

The noise of a measurement chain designed to measure very low microwave signals is one of its key characteristics. As such, amplifiers in this chain, and especially the first one,

which will often determine the noise figure of the full chain, should add as little noise as possible. Quantum mechanics states that at least half a photon of noise, i.e. an energy of $\frac{\hbar\omega}{2}$, will be added for each additional mode involved in the amplification process. In a perfect Josephson parametric amplifier, working in a phase-preserving mode, one can then expect a minimal added noise level of $\frac{\hbar\omega}{2}$, because of the presence of the idler mode. This is the standard quantum limit (SQL) and corresponds to a noise temperature of about 145 mK at a frequency of 6 GHz.

We have seen previously that our device presents some internal losses, especially at strong pump power (nonlinear losses) which means that energy is transferred to other modes. In principle this coupling to other modes, if large enough, could degrade the noise figure of the amplifier as these modes will inject their vacuum noise into the amplifier [23]. In this case, the resulting noise is expected to be increased by a factor $\frac{\gamma_1+\gamma_{\mathrm{tot}}}{\gamma_1}$, where γ_{tot} is the total internal loss rate. In our case, considering the internal losses of the device, we thus expect this mechanism to enhance the noise by about 10% above the SQL. We measure the noise of the amplifier using a shot noise tunnel junction (SNTJ), which serves as a self calibrated broadband noise source when voltage-biased (see Extended Data Fig. 3 and supplementary information, section I, for details about the setup) and replaces the VNA input tone. The broadband SNTJ output is amplified by the device and we measure the resulting signal with a spectrum analyzer. Studying the power spectral density of the output signal as a function of the SNTJ bias voltage, we are able to extract, for each frequency, the system gain and the noise added by the system (see supplementary information, section VI). In Fig. 4b and c, we present the frequency dependence of the fitted gain and added noise, when the amplifier is set to operate at a center frequency of 6.13 GHz. We see that there is a clear anticorrelation between the two. When the gain of the parametric amplifier is low, the noise added by the system is, as expected, close to 15 photons. It is limited by the noise of the High Electron Mobility Transistor (HEMT) amplifier thermalized at 4 K and additional losses in the system. When the gain of the amplifier increases, getting closer to the pump frequency, the system added noise decreases dramatically and reaches a value close to the SQL. The fact that the full system does not quite reach the SQL is mainly due to the limited gain in the accessible measurement range (see Extended Data Fig. 4 and supplementary information, section VI). Because the setup does not allow to measure the noise very close to the pump frequency, the gain is limited to about 15 dB which is not

enough to overcome the HEMT noise on the next amplification stage. We can thus conclude that our graphene based Josephson parametric amplifier adds a minimal amount of noise, set by quantum mechanics, which is comparable to the state of the art of quantum limited amplifiers. In this regard it compares favourably to traveling wave parametric amplifiers. In such amplifier, which has the advantage of intrinsically presenting a very large amplification bandwidth, the reported noise are typically limited to about twice the SQL [24].

In conclusion, we have demonstrated a Josephson parametric amplifier using an electric field tunable Josephson junction made of graphene. The amplification bandwidth of the device is tunable over about 1 GHz with a simple electric field in addition to presenting a gain > 20 dB and noise close to the standard quantum limit. This experimental demonstration of a gate-tunable semiconductor weak-link Josephson parametric amplifier opens interesting perspectives for different amplification schemes. For example, pumping the gate voltage at twice the signal frequency would modify the critical current and thus directly modulate the kinetic inductance. In practice such scheme should produce a three wave mixing amplification process, similar to flux pumping in SQUID based Josephson parametric amplifiers [25]. The three wave mixing process, which has the advantage of frequency separation between signal and pump, could also be observed in graphene based Josephson parametric amplifier using other strategies. The possibility to bias the junction with a DC current, as is demonstrated in this work, could naturally give access to the nonlinearity necessary to achieve three wave mixing [26]. In addition, in Josephson junctions presenting a non sinusoidal current phase relation, which has been reported in graphene [17, 18], three wave mixing terms are present even at zero DC current bias and could be directly used. Together with the recent developments regarding qubits [27], bolometers [28, 29] and the use of van der Waals materials in superconducting quantum circuits [30, 31], the demonstration we report here for quantum limited amplifiers, and the related work of Sarkar et al. [32], position semiconductor based Josephson junctions as key elements for future integrated superconducting quantum circuits.

Acknowledgments

We thank José Aumentado and Florent Lecocq (National Institute of Standards and Technology, Boulder, Colorado, USA) for providing the SNTJ and for discussions. This

work was supported by the French National Research Agency (ANR) in the framework of the Graphmon project (ANR-19-CE47-0007). K.W. and T.T. acknowledge support from JSPS KAKENHI (Grant Numbers 19H05790, 20H00354 and 21H05233). JR acknowledges E. Eyraud and W. Wernsdorfer for help with the cryogenic system. We acknowledge the work of J. Jarreau, L. Del-Rey and D. Dufeu for the design and fabrication of the sample holders and other mechanical pieces used in the cryogenic system. We thank the Nanofab group at Institut Néel for help with devices fabrication. We thank K. W. Murch and B. Sacépé for discussions and comments on the manuscript.

Author contributions statement

K. W. and T. T. grew the h-BN crystals. G. B. and J. R. designed the samples. G. B. and N. A. fabricated the devices. G. B., A. J. and J. R. performed DC measurements. G. B. performed the microwave measurements with help from K. R. A. and J. R. Noise measurements were realized by G. B., A. R. and M. E. with help from N. R. and J. R. Data analysis was performed by G. B. with help from A. R., N. R. and J. R. The project was supervised by F. L. and J. R. G.B. prepared the figures of the manuscript. J. R. wrote the manuscript with input from all authors.

Competing interests statement

N.R. is founder and shareholder of Silent Waves.

Figures captions

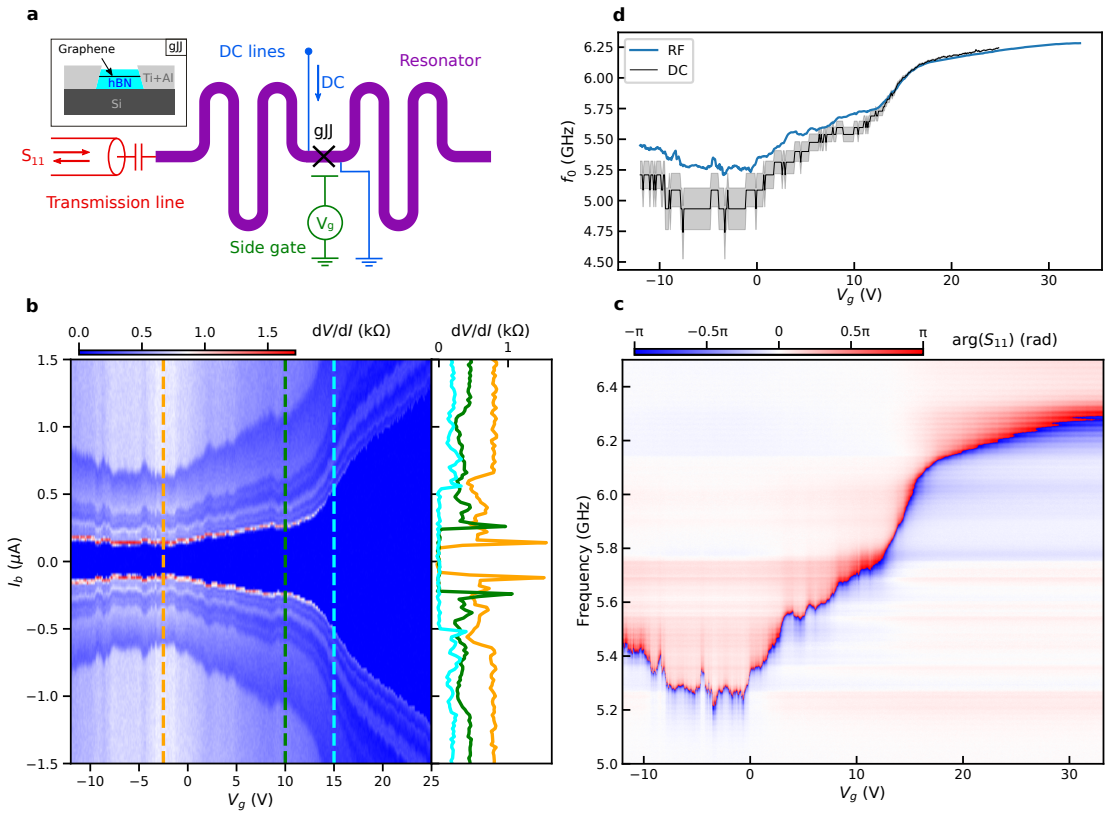

Figure 1. Graphene Josephson junction embedded in a microstrip superconducting microwave resonator. (a): Device geometry. The system is probed in reflection (S_{11} scattering parameter) via a radiofrequency (RF) transmission line connected to the resonator with a coupling capacitor. The graphene Josephson junction (gJJ) is located in the center of the resonator. Additional lines allow for DC measurements. A voltage V_g on the side gate tunes the carrier concentration in the gJJ. In the inset, a cross-section of the gJJ illustrates the side contacts with Ti/Al on the h-BN encapsulated graphene. (b): Differential resistance ($\frac{dV}{dI}$) of the gJJ as a function of V_g and the bias current I_b. The blue region represents the dissipation-less regime, i.e. below the junction critical current. The critical current depends on the carrier concentration, controlled by V_g, and is smaller near the Dirac point at $V_g \approx -3\ V$. Linecuts at different gate voltages (right) are used to determine the evolution of the critical current with gate voltage. (c): Phase of the S_{11} parameter as a function of gate voltage and microwave frequency. The resonance appears as a 2π phase shift as a function of frequency. (d): Comparison of the resonance frequency extracted from microwave reflection (c) (blue solid lines) and the one predicted from the change of Josephson inductance inferred from the critical current (b) (grey line). The error bands stem from the current bias digitization steps that lead to uncertainty in the determination of the critical current (see supplementary information, section IV). Voltage sweeps were made towards positive voltages because of an hysteretic behaviour that we attribute to the use of a side gate (see supplementary information, section III).

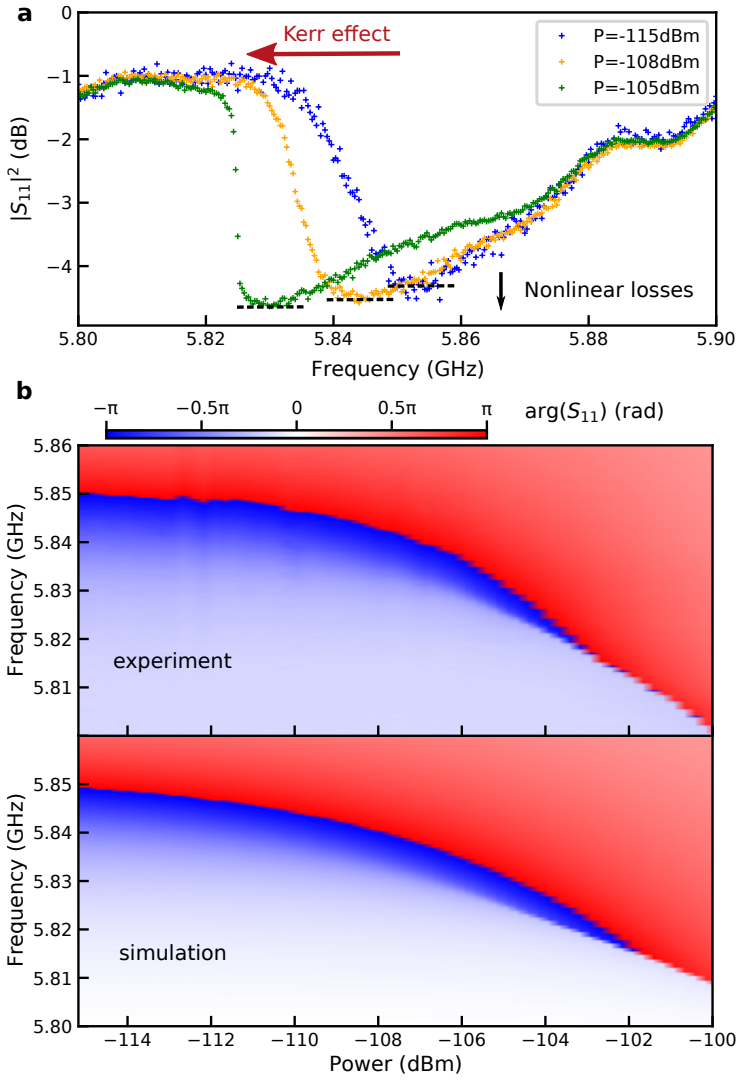

Figure 2. Nonlinearity of a microwave resonator with an embedded graphene Josephson junction. Measurements of the frequency dependance of the microwave reflection magnitude ($|S_{11}|^2$) for different input powers (a). The resonance frequency shifts to lower frequencies (Kerr effect) and the reflection dip increases (nonlinear losses). The measurements are performed at V_g=15 V corresponding to a resonance frequency of ≈5.85 GHz in the low power regime. Measurements are made by scanning the microwave frequency from low to high, at a fixed VNA power and then changing the power. (b): comparison of the measured microwave reflection (phase) with the predictions of a minimal model presented in the text. The power evolution of the resonance is captured by the simple model of Eq. 1 (see text and supplementary information, section V) and gives us access to the following parameters: a low power resonance frequency $\frac{\omega_r}{2\pi}$=5.849 GHz, an external (resp. internal) energy damping rate $2\gamma_1=2\pi\times22.0$ MHz (resp. $2\gamma_2=2\pi\times1.90$ MHz), a Kerr coefficient K=-$2\pi\times135$ kHz and nonlinear damping rate $2\gamma_3=2\pi\times22$ kHz.

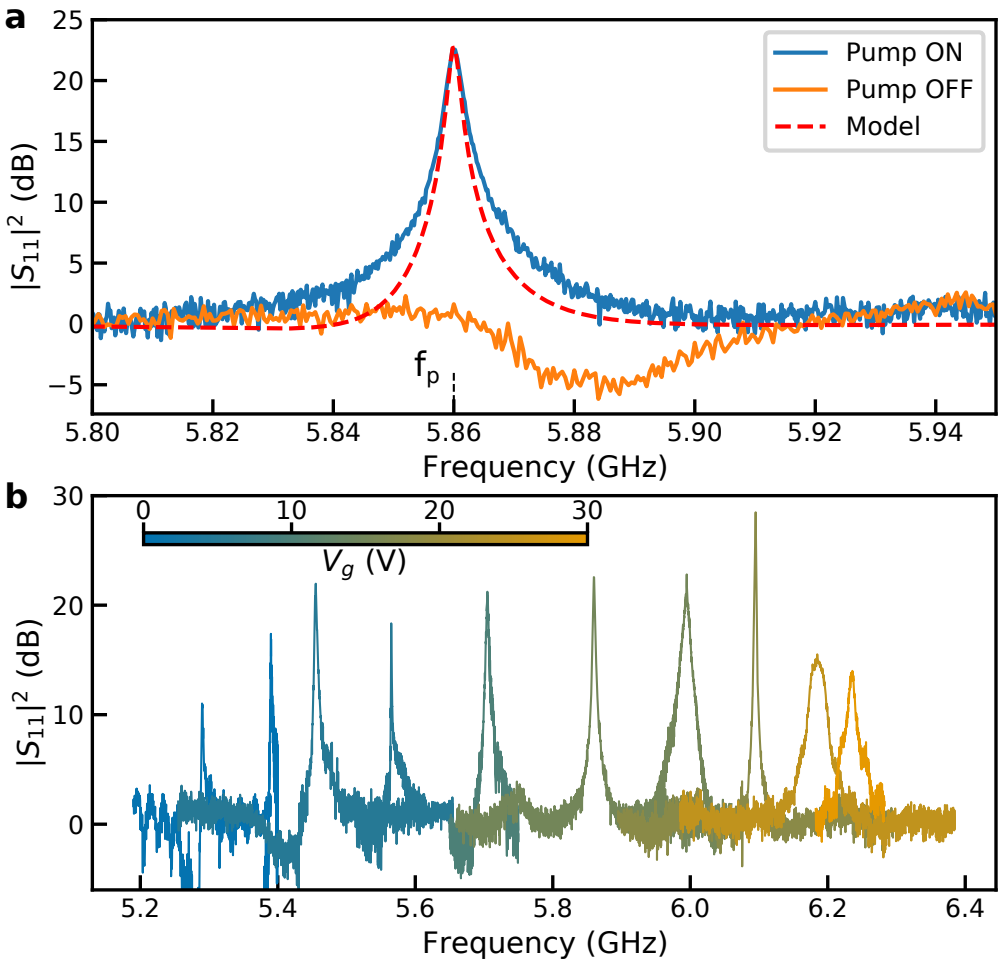

Figure 3. Parametric amplification in a microwave resonator with an embedded graphene Josephson junction. (a): Effect of the pump on the microwave reflection magnitude ($|S_{11}|^2$). The gate voltage is set at V_g=15 V. In absence of the pump (orange solid line, pump OFF), a dip appears at the resonance frequency. In presence of a pump at f_p, the reflected signal shows a strong gain, up to 22 dB (blue solid line, pump ON). The measured gain is compared to the one predicted with the minimal model of parametric amplification presented in the text using the resonator parameters extracted from a one-tone measurement, a pump frequency f_p= 5.860 GHz and a pump power of 95% of the critical power, corresponding experimentally to -103 dBm. A slight shift in the resonator frequency, due to an instability in the gate voltage, compared to the setpoint of Fig. 2 resulted in a modified ω_r=2$\pi\times$ 5.885 GHz and Kerr coefficient K=-2$\pi\times$ 111 kHz, all other parameters were kept constant. (b): Gate voltage tuning of the amplifier. The resonance frequency is tuned with V_g and allows gain in a different frequency windows close to the resonance frequency by optimizing pump power and frequency for each V_g. Values of V_g (from left to right): 0.5 V, 0 V, 5 V, 5 V, 10 V, 15 V, 15 V, 18 V, 25 V, 30 V. The nonmonotonous trend and the fact that the some gate voltages appear twice with different frequencies come from charge instabilities (see supplementary information, section III).

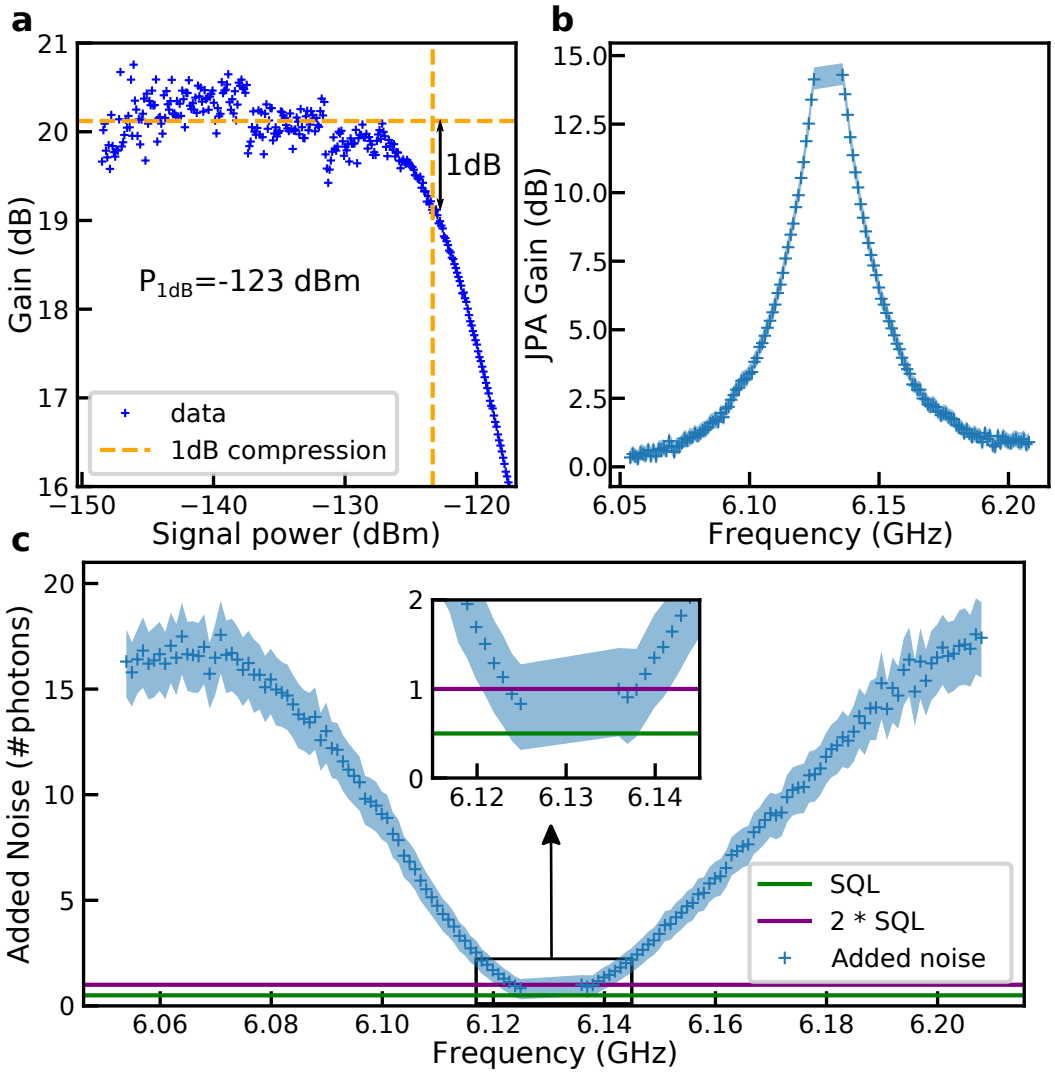

Figure 4. Performance of the resonant Josephson parametric amplifier. (a): Signal power dependance of the gain showing a 1 dB compression point P_{1dB}=-123 dBm for a gain of 20 dB at a working frequency of 6.13 GHz. (b): Gain of the amplifier measured with the SNTJ and the spectrum analyzer. The shaded area represents the error band (standard deviation) in the fitting procedure used to extract the gain, see supplementary information, section VI. (c): Demonstration of noise close to the standard quantum limit (SQL). The device is set such that the gain is 20 dB at 6.13 GHz (pump frequency). Away from the center of the amplification window of the device, the added noise is about 15 photons, mainly set by the HEMT amplifier at the 4 K stage. When the gain of the parametric amplifier increases, the added noise decreases and reaches values close to the standard quantum limit. Analysis is not possible at the very center of the amplification band due to the presence of the pump. The shaded area represents the error band in the determination of the added noise (see supplementary information, section VI). It is mostly due to the uncertainty on the SNTJ temperature (standard deviation), see supplementary information, section VI.

References

[1] R. J. Schoelkopf and S. M. Girvin, Wiring up quantum systems, Nature **451**, 664 (2008).

[2] M. A. Castellanos-Beltran and K. W. Lehnert, Widely tunable parametric amplifier based on a superconducting quantum interference device array resonator, Applied Physics Letters **91**, 10.1063/1.2773988 (2007), arXiv:0706.2373.

[3] M. A. Castellanos-Beltran, K. D. Irwin, G. C. Hilton, L. R. Vale, and K. W. Lehnert, Amplification and squeezing of quantum noise with a tunable Josephson metamaterial, Nature Physics **4**, 929 (2008), arXiv:0806.0659.

[4] R. Vijay, D. H. Slichter, and I. Siddiqi, Observation of Quantum Jumps in a Superconducting Artificial Atom, Physical Review Letters **106**, 110502 (2011), arXiv:1009.2969.

[5] J. D. Teufel, T. Donner, M. A. Castellanos-Beltran, J. W. Harlow, and K. W. Lehnert, Nanomechanical motion measured with an imprecision below that at the standard quantum limit, Nature Nanotechnology **4**, 820 (2009).

[6] T. Walter, P. Kurpiers, S. Gasparinetti, P. Magnard, A. Potočnik, Y. Salathé, M. Pechal, M. Mondal, M. Oppliger, C. Eichler, and A. Wallraff, Rapid High-Fidelity Single-Shot Dispersive Readout of Superconducting Qubits, Physical Review Applied **7**, 054020 (2017).

[7] K. M. Backes, D. A. Palken, S. A. Kenany, B. M. Brubaker, S. B. Cahn, A. Droster, G. C. Hilton, S. Ghosh, H. Jackson, S. K. Lamoreaux, A. F. Leder, K. W. Lehnert, S. M. Lewis, M. Malnou, R. H. Maruyama, N. M. Rapidis, M. Simanovskaia, S. Singh, D. H. Speller, I. Urdinaran, L. R. Vale, E. C. van Assendelft, K. van Bibber, and H. Wang, A quantum enhanced search for dark matter axions, Nature **590**, 238 (2021).

[8] G. de Lange, B. van Heck, A. Bruno, D. J. van Woerkom, A. Geresdi, S. R. Plissard, E. P. A. M. Bakkers, A. R. Akhmerov, and L. DiCarlo, Realization of Microwave Quantum Circuits Using Hybrid Superconducting-Semiconducting Nanowire Josephson Elements, Physical Review Letters **115**, 127002 (2015), arXiv:1503.08483.

[9] T. W. Larsen, K. D. Petersson, F. Kuemmeth, T. S. Jespersen, P. Krogstrup, J. Nygård, and C. M. Marcus, Semiconductor-Nanowire-Based Superconducting Qubit, Physical Review Letters **115**, 127001 (2015), arXiv:1503.08339.

[10] L. Casparis, M. R. Connolly, M. Kjaergaard, N. J. Pearson, A. Kringhøj, T. W. Larsen, F. Kuemmeth, T. Wang, C. Thomas, S. Gronin, G. C. Gardner, M. J. Manfra, C. M. Marcus, and K. D. Petersson, Superconducting gatemon qubit based on a proximitized two-dimensional electron gas, Nature Nanotechnology **13**, 915 (2018), arXiv:1711.07665.

[11] M. Mergenthaler, A. Nersisyan, A. Patterson, M. Esposito, A. Baumgartner, C. Schönenberger, G. A. D. Briggs, E. A. Laird, and P. J. Leek, Circuit Quantum Electrodynamics with Carbon-Nanotube-Based Superconducting Quantum Circuits, Physical Review Applied **15**, 064050 (2021).

[12] F. E. Schmidt, M. D. Jenkins, K. Watanabe, T. Taniguchi, and G. A. Steele, A ballistic graphene superconducting microwave circuit, Nature Communications **9**, 4069 (2018), arXiv:1806.11389.

[13] J. I. Wang, D. Rodan-Legrain, L. Bretheau, D. L. Campbell, B. Kannan, D. Kim, M. Kjaergaard, P. Krantz, G. O. Samach, F. Yan, J. L. Yoder, K. Watanabe, T. Taniguchi, T. P. Orlando, S. Gustavsson, P. Jarillo-Herrero, and W. D. Oliver, Coherent control of a hybrid superconducting circuit made with graphene-based van der Waals heterostructures, Nature Nanotechnology **14**, 120 (2019), arXiv:1809.05215.

[14] P. Sikivie, Invisible axion search methods, Rev. Mod. Phys. **93**, 015004 (2021).

[15] H. Zimmer, Parametric amplification of microwaves in superconducting josephson tunnel junctions, Applied Physics Letters **10**, 193 (1967), https://doi.org/10.1063/1.1754906.

[16] J. Park, J. H. Lee, G.-H. Lee, Y. Takane, K.-I. Imura, T. Taniguchi, K. Watanabe, and H.-J. Lee, Short Ballistic Josephson Coupling in Planar Graphene Junctions with Inhomogeneous Carrier Doping, Physical Review Letters **120**, 077701 (2018).

[17] G. Nanda, J. L. Aguilera-Servin, P. Rakyta, A. Kormányos, R. Kleiner, D. Koelle, K. Watanabe, T. Taniguchi, L. M. K. Vandersypen, and S. Goswami, Current-phase relation of ballistic graphene josephson junctions, Nano Letters **17**, 3396 (2017), pMID: 28474892, https://doi.org/10.1021/acs.nanolett.7b00097.

[18] F. E. Schmidt, M. D. Jenkins, K. Watanabe, T. Taniguchi, and G. A. Steele, Probing the current-phase relation of graphene josephson junctions using microwave measurements (2020), arXiv:2007.09795 [cond-mat.mes-hall].

[19] R. Haller, G. Fülöp, D. Indolese, J. Ridderbos, R. Kraft, L. Y. Cheung, J. H. Ungerer, K. Watanabe, T. Taniguchi, D. Beckmann, R. Danneau, P. Virtanen, and C. Schö-

nenberger, Phase-dependent microwave response of a graphene Josephson junction (2021), arXiv:2108.00989.

[20] B. Yurke and E. Buks, Performance of Cavity-Parametric Amplifiers, Employing Kerr Nonlinearites, in the Presence of Two-Photon Loss, Journal of Lightwave Technology **24**, 5054 (2006), arXiv:0505018 [quant-ph].

[21] J. Y. Mutus, T. C. White, E. Jeffrey, D. Sank, R. Barends, J. Bochmann, Y. Chen, Z. Chen, B. Chiaro, A. Dunsworth, J. Kelly, A. Megrant, C. Neill, P. J. J. O'Malley, P. Roushan, A. Vainsencher, J. Wenner, I. Siddiqi, R. Vijay, A. N. Cleland, and J. M. Martinis, Design and characterization of a lumped element single-ended superconducting microwave parametric amplifier with on-chip flux bias line, Applied Physics Letters **103**, 122602 (2013), arXiv:1308.1376.

[22] L. Planat, R. Dassonneville, J. P. Martínez, F. Foroughi, O. Buisson, W. Hasch-Guichard, C. Naud, R. Vijay, K. Murch, and N. Roch, Understanding the Saturation Power of Josephson Parametric Amplifiers Made from SQUID Arrays, Physical Review Applied **11**, 034014 (2019), arXiv:1809.08476.

[23] C. Eichler and A. Wallraff, Controlling the dynamic range of a Josephson parametric amplifier, EPJ Quantum Technology **1**, 2 (2014).

[24] C. Macklin, K. O'Brien, D. Hover, M. E. Schwartz, V. Bolkhovsky, X. Zhang, W. D. Oliver, and I. Siddiqi, A near quantum-limited josephson traveling-wave parametric amplifier, Science **350**, 307 (2015), https://www.science.org/doi/pdf/10.1126/science.aaa8525.

[25] T. Yamamoto, K. Inomata, M. Watanabe, K. Matsuba, T. Miyazaki, W. D. Oliver, Y. Nakamura, and J. S. Tsai, Flux-driven Josephson parametric amplifier, Applied Physics Letters **93**, 042510 (2008), arXiv:0808.1386.

[26] M. R. Vissers, R. P. Erickson, H.-S. Ku, L. Vale, X. Wu, G. C. Hilton, and D. P. Pappas, Low-noise kinetic inductance traveling-wave amplifier using three-wave mixing, Applied Physics Letters **108**, 012601 (2016), https://doi.org/10.1063/1.4937922.

[27] T. W. Larsen, M. E. Gershenson, L. Casparis, A. Kringhøj, N. J. Pearson, R. P. G. McNeil, F. Kuemmeth, P. Krogstrup, K. D. Petersson, and C. M. Marcus, Parity-protected superconductor-semiconductor qubit, Phys. Rev. Lett. **125**, 056801 (2020).

[28] G.-H. Lee, D. K. Efetov, W. Jung, L. Ranzani, E. D. Walsh, T. A. Ohki, T. Taniguchi, K. Watanabe, P. Kim, D. Englund, and K. C. Fong, Graphene-based Josephson junction microwave bolometer, Nature **586**, 42 (2020), arXiv:1909.05413.

[29] R. Kokkoniemi, J.-P. Girard, D. Hazra, A. Laitinen, J. Govenius, R. E. Lake, I. Sallinen, V. Vesterinen, M. Partanen, J. Y. Tan, K. W. Chan, K. Y. Tan, P. Hakonen, and M. Möttönen, Bolometer operating at the threshold for circuit quantum electrodynamics, Nature **586**, 47 (2020), arXiv:2008.04628.

[30] A. Antony, M. V. Gustafsson, G. J. Ribeill, M. Ware, A. Rajendran, L. C. G. Govia, T. A. Ohki, T. Taniguchi, K. Watanabe, J. Hone, and K. C. Fong, Miniaturizing transmon qubits using van der waals materials, Nano Letters **21**, 10122 (2021), pMID: 34792368, https://doi.org/10.1021/acs.nanolett.1c04160.

[31] J. I. Wang, M. A. Yamoah, Q. Li, A. H. Karamlou, T. Dinh, B. Kannan, J. Braumüller, D. Kim, A. J. Melville, S. E. Muschinske, B. M. Niedzielski, K. Serniak, Y. Sung, R. Winik, J. L. Yoder, M. E. Schwartz, K. Watanabe, T. Taniguchi, T. P. Orlando, S. Gustavsson, P. Jarillo-Herrero, and W. D. Oliver, Hexagonal boron nitride as a low-loss dielectric for superconducting quantum circuits and qubits, Nature Materials 10.1038/s41563-021-01187-w (2022), arXiv:2109.00015.

[32] J. Sarkar, K. V. Salunkhe, S. Mandal, S. Ghatak, A. H. Marchawala, I. Das, K. Watanabe, T. Taniguchi, R. Vijay, and M. M. Deshmukh, Quantum noise limited microwave amplification using a graphene josephson junction (2022), arXiv:2204.02103.

Methods

Devices fabrication

We use a van der Waals heterostructure made of graphene encapsulated in hexagonal boron nitride (h-BN), connected to two superconducting leads (Ti/Al) to build the Josephson junction. h-BN encapsulation and one dimensional side contacts ensure high charge carrier mobility and low contact resistance which are both needed for reaching large critical currents. The h-BN encapsulated graphene stacks were made using a polymer-free assembly technique [33] on a high-resistivity Si substrate. Devices were processed with 2 steps of e-beam lithography (80 kV) using positive resists (PMMA) and an additional layer of conductive resist for the contact step (AllResist/Electra). The first step allows to expose all the elements of the device (transmission line, resonator, DC lines and gate) and is followed by an etching step giving access to the graphene edges. Etching was performed using reactive ion etching and a mixture of O_2 and CHF_3. Right after the etching step, the sample is

installed into the e-beam evaporation chamber for metal deposition (Ti/Al; 5 nm/60 nm). The second lithography step is also followed by an etching step and allows to define the shape of the gJJ and separate it from the side gate. The size of the gJJ is 300 nm between the superconducting contacts and 1.5 μm in the transverse direction.

Design of the resonator

The schematic of the device is shown in Extended Data Fig. 1. The external quality factor was set by design (i.e. coupling capacitance) with the help of electromagnetic simulations. We target a value of 100 which is typical for a resonant JPA. Experimentally, we measured external quality factors in the range 100 to 200 depending on the resonance frequency because of variations in the environment impedance. The internal quality factor was measured in different configurations. In a design with higher external quality factor, we checked that the use of a Ti layer was not a limiting factor and measured internal quality factors in the range 2000 to 10000. In the amplifier design, we measured that the bare internal quality factor, i.e. without the graphene junction, was >1000. In the presence of the junction, this was reduced to lower values (400-1000 depending on the frequency, with the lower values being measured close to the neutrality point) which indicates that the junction has some non-negligeable losses. Nevertheless, since the internal quality factor remains above the external one, we expect a limited effect on the added noise.

A side gate allows to control the carrier density in the graphene junction. We chose to use a side gate instead of a traditional backgate or topgate in order to limit potential sources of loss. State of the art backgate are indeed usually done with a graphite flake. Graphite is a normal metal and could, in principle, introduce some losses that would have an effect on the amplifier added noise. Side gating results in charge inhomogeneity which in turn results in a reduced gating efficiency. This explains why the neutrality point is not sharply defined in Fig. 1b and why the associated resistance peak in the normal state appears broad (see Extended Data Fig. 2 and Supplementary information, section IV).

DC and Microwave measurements

Measurements were performed in dilution refrigerators with base temperatures of 25 mK. The resonator is probed at microwave frequencies in a reflection geometry. The scattering parameter S_{11} is measured while additional probes allow us to characterize the junction low-frequency (DC) properties. The position of those probes, close to center of the resonator, was chosen in order to minimize their effect on the microwave properties and in particular any microwave leakage. DC measurements were performed using low frequency lock-in techniques. We have removed a constant baseline resistance of 1207 Ω from the 2 probe measurement. This corresponds to the resistance of the measurement wires. The microwave measurement setup is presented in details in Extended Data Fig. 3 and in the Supplementary Information, section I. One tone microwave measurements were performed with a vector network analyzer. Two-tone measurements (for instance to measure the amplifier gain) were performed using an additional microwave source. The reflected signal is split with a circulator or a directionnal coupler depending on the setup and amplified at 4 K and again at room temperature. For noise measurement the signal is measured with a spectrum analyzer using a resolution bandwidth of 2 MHz (3 dB bandwidth).

Influence of the SNTJ packaging attenuation on the added noise estimation

The attenuation between the SNTJ and the gJPA was not taken into account in the added noise fitting procedure (see Supplementary Information, section VI). This has the effect of overestimating the intrinsic noise added by the gJPA. We estimate the total attenuation in between the SNTJ and the gJPA to be 2.2 dB meaning that the fitted intrinsic added noise by the gJPA is 2.2 dB higher than its real value. For example, the minimum added noise measured is 0.8 photon including 0.5 photon coming from the vacuum noise in the idler channel. It means that the corrected intrinsic added noise by the gJPA is reduced by 2.2 dB from the measured 0.3 photon value, making the total added noise 0.68 photon instead of 0.8 photon.

Data Availability

The data that support the findings of this study are available in Zenodo with the identifier https://doi.org/10.5281/zenodo.7025633

Methods-only references

[33] L. Wang, I. Meric, P. Y. Huang, Q. Gao, Y. Gao, H. Tran, T. Taniguchi, K. Watanabe, L. M. Campos, D. A. Muller, J. Guo, P. Kim, J. Hone, K. L. Shepard, and C. R. Dean, One-Dimensional Electrical Contact to a Two-Dimensional Material, Science (New York, N.Y.) **342**, 614 (2013), arXiv:1005.4917.